# We are IntechOpen,
# the world's leading publisher of
# Open Access books
# Built by scientists, for scientists

## 4,800
Open access books available

## 122,000
International authors and editors

## 135M
Downloads

## 154
Countries delivered to

Our authors are among the

## TOP 1%
most cited scientists

## 12.2%
Contributors from top 500 universities

**WEB OF SCIENCE**™

Selection of our books indexed in the Book Citation Index
in Web of Science™ Core Collection (BKCI)

## Interested in publishing with us?
## Contact book.department@intechopen.com

Numbers displayed above are based on latest data collected.
For more information visit www.intechopen.com

# Impact Response of Nanofluid-Reinforced Antiballistic Kevlar Fabrics

Roberto Pastore, Giorgio Giannini,
Ramon Bueno Morles, Mario Marchetti and
Davide Micheli

Additional information is available at the end of the chapter

## 1. Introduction

In the last decades the research on composite materials have been acquiring importance due to the possibility of increasing the material mechanical performances while contemporary decreasing both mass and volume of the structures. Mass lowering is a "must" especially in military and space applications, since aircraft aerodynamic profile needs to be optimized and because of the high costs of launch and launcher and payload mass constraints [1]. The need to face up to the well know problem of the so called "space debris" has led many aerospace researchers to look for advanced lightweight materials for ballistic applications. Among all innovative materials, a promising branch of such research focuses on the polymeric composite materials with inclusions of nanostructures [2]. The present work fits in a more general research project, the aim of which is to realize, study and characterize nanocomposite materials. These latter are currently manufactured in the SASLab of Astronautic Engineering Department of University of Rome "Sapienza" *(www.saslab.eu)* by mixing the nanoparticles within polymeric matrixes in such a way to obtain a material as homogeneous as possible, in order to have a final composite with improved physical characteristic [3]. The goal of the present study is to perform a ballistic characterization of the nanocomposites by means of an in-house built electromagnetic accelerator. The realization of such experimental apparatus, and mostly the optimization with a view to space debris testing planes, is quite complex since the fundamental machine parameters have high non-linearity theoretical behavior [4]. Hereafter experimental preliminary results of a prototypal device are presented and discussed. An intriguing issue of nanoscience research for aerospace applications is to produce a new thin, flexible, lightweight and inexpensive material that have an equivalent

or even better ballistic properties than the existing Kevlar fabrics. A shear thickening fluid (STF) is a material with remarkable properties [5]. STFs are very deformable materials in the ordinary conditions and flow like a liquid as long as no force is applied. However they turn into a very rigid solid-like material at high shear rates. Shear thickening is a non-newtonian fluid behavior defined as the increase of viscosity with the increase in the applied shear rate. This phenomenon can occur in micro/nano colloidal dispersions. More concentrated colloidal suspensions have been shown to exhibit reversible shear thickening resulting in large, sometimes discontinuous, increases in viscosity above a critical shear rate. Two main causes of reversible shear thickening have been proposed: the order-disorder transition and the "hydrocluster" mechanism. This transition from a flowing liquid to a solid-like material is due to the formation and percolation of shear induced transient aggregates, or hydroclusters, that dramatically increase the viscosity of the fluid. Support for such mechanism has been demonstrated experimentally through rheological, rheo-optics and flow-SANS experiments as well as computer simulation. It has been reported in the literature that shear thickening has been observed for a wide variety of suspensions such as clay-water, calcium carbonate-water, polystyrene spheres in silicon oil, iron particles in carbon tetrachloride, titanium dioxide-resin, silica-polypropylene glycol, and silica-ethylene glycol. The phenomenon of shear thickening of suspensions in general has no useful applications in industrial production. Recently Wagner's group and U.S. Army research lab developed a body armor using shear thickening fluid and Kevlar fabric [6]. These research results demonstrate that ballistic penetration resistance of Kevlar fabric is enhanced by impregnation of the fabric with a colloidal STF. Impregnated STF/fabric composites are shown to provide superior ballistic protection as compared with simple stacks of neat fabric and STF. Comparisons with fabrics impregnated with non-shear thickening fluids show that the shear thickening effect is critical to achieving enhanced performance. Many researchers have used various techniques to prepare the STFs. Acoustic cavitations technique is one of the efficient ways to disperse nanoparticles into the liquid polymers. In this case, the application of alternating acoustic pressure above the cavitations threshold creates numerous cavities in the liquid. Some of these cavities oscillate at a frequency of the applied field (usually 20 kHz) while the gas content inside these cavities remains constant. However, some other cavities grow intensely under tensile stresses while yet another portion of these cavities, which are not completely filled with gas, starts to collapse under the compression stresses of the sound wave. In the latter case, the collapsing cavity generates tiny particles of 'debris' and the energy of the collapsed one are transformed into pressure pulses. It is noteworthy that the formation of the debris further facilitates the development of cavitation. It is assumed that acoustic cavitations in liquids develop according to a chain reaction. Therefore, individual cavities on real nuclei are developing so rapidly that within a few microseconds an active cavitations region is created close to the source of the ultrasound probe. The development of cavitations processes in the ultrasonically processed melt creates favorable conditions for the intensification of various physical-chemical processes. Acoustic cavitations accelerate heat and mass transfer processes such as diffusion, wetting, dissolution, dispersion, and emulsification. SASLab objective in this research field is to synthesize a STF in a single step reaction through high power ultrasound technique, fabricate STF/fabric composite and characterize

it for ballistic resistance applications. The STF is a combination of silicon dioxide (silica) nanoparticles suspended in a liquid polymer. This mixture of flowable and hard components at a particular composition results in a material with remarkable properties. The STF is prepared by ultrasound irradiation of silica nanoparticles dispersed in liquid polyethylene glycol polymer. The as-prepared STFs are then tested for their rheological properties. Kevlar fabrics are soaked in STF/ethanol solution to make STF/fabric composite. Ballistic tests are performed on the neat fabrics and STF/fabric composite targets. The results show that STF impregnated fabrics have better penetration resistance as compared to neat fabrics, without affecting the fabric flexibility. That indicates that the STF addition to the fabric may enhance the fabric performance and thus can be used for ballistic applications.

## 2. Materials manufacturing and characterization

In this section the procedures adopted for the shear thickening nanofluids realization and the Kevlar-reinforced fabrics manufacturing are basically described, providing rheological and morphological (SEM *TESCAN-Vega LSH*, Large Stage High Vacuum scanning electron microscope) characterization of the materials under testing too. Silica nanoparticles (n-$SiO_2$, *Sigma Aldrich* Fumed Silica powder 0.007μm) and Polyethylene glycol (PEG, *Sigma Aldrich* Poly(ethylene glycol) average mol wt 200) have been chosen as nanofiller and carrier fluid respectively, to follow the tracks of the most remarkable results in STF applications for absorbing impact energy [6-8]. Ethanol (*Sigma Aldrich* Ethanol puriss. p.a., ACS reagent) was used as solvent for nanopowder disentanglement and dispersion within the polymeric matrix. SEM images of the as-received silica nanoparticles are shown in Figure 1 below.
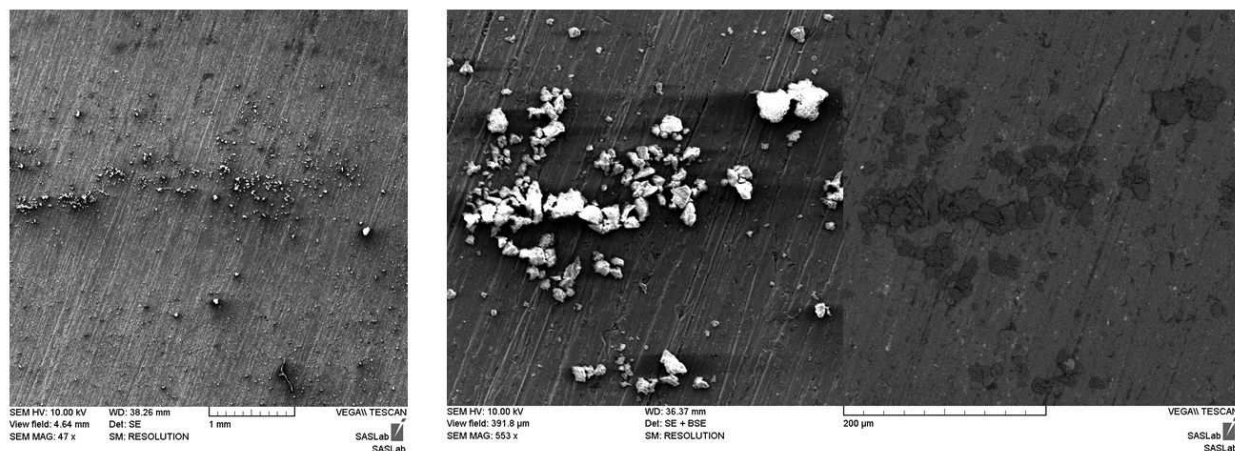


**Figure 1.** Low (left) and medium (right) magnification SEM photos of the silica nanoparticles adopted; the BSE image enhances the high degree of the as-received material homogeneity.

Several are the parameters of the procedure for the solution preparation and, moreover, their combination greatly affects the efficacy of the later fabrics impregnation (i.e. the effective nanofluid amount intercalated between the fibers) as well as the ballistic behavior of the

final manufactured test article. Mixing tools are fundamental to achieve a correct preparation of the nanostructured solution, since a suitable nanoparticles dispersion inside the liquid matrix and the subsequent mixture homogenization are absolutely not trivial tasks, in particular in case (as the present) of substantial filler weight percentages. Nanopowders very high "surface area" (surface/weight ratio, in the case of the adopted nanoparticles the value 390 m$^2$/g is reported in the data sheet) give rise to so huge volumetric gaps between the host fluid and the filler (dry nanopowder volume may be one order of magnitude greater than the matrix volume). Beside the dilution in organic solvent (which must be used in controlled excess to avoid the whole mixture degradation) a first mechanical mixing (performed by *Velp Scientifica* Magnetic Stirrer BS Type 0÷2000rpm) to gradually introduce the nanoparticles in solution is needed. Then, 20kHz ultrasonication technique (by *Sonics & Materials* VC 750 Ultrasonic Liquid Processor) is adopted to exfoliate the micrometric agglomerates in which the nanoparticles are typically entangled, in order to increase the mixture homogeneity as well as to reduce the presence of internal air voids. During this step an increase by several tens degrees of the solution temperature may occur, due to the relatively high energy quantities exchanged: as each case requires (i.e. depending on parameters as solvent amount, evaporation rate, compound thermal stability, etc.) the sonication can be carried out in thermostatic environment or not. Of course, the timing procedure strictly depends on the material quantities utilized, which in turn are linked to the characteristics (surface dimensions and absorption rate) of the specific fabric typology treated. Schematically, the method for the preparation of by about 120g of nanofluid loaded at 20wt%, an amount estimated to perform the full treatment of eleven 16×16cm layers of reference batavia Kevlar fabric (see below) consists of the following steps: 60g of PEG mechanical 500rpm mixing in 200÷300ml of solvent for about 10 minutes, gradual addition of 12g of silica nanoparticles, high energy ultrasonication (50% of mixer maximum power) for about 30 minutes, low energy ultrasonication (25% of mixer maximum power) for about 4 hours in low temperature (0÷5 C) environment, and low energy ultrasonication for about 2 hours in warming temperature (up to 50 C). The result of such procedure is an homogeneous solution of volume reduced to 80÷120ml, mainly due to the evaporation of a certain amount of solvent as well as to the nanoparticles/polymeric macromolecules coupling inside the solution (testified by an evident chromatic transition from opaque to quasi-transparent solution). Whereas the next step for the fabric-reinforced manufacture should be the fabric impregnation in the solution (followed by the total evaporation of the solvent in excess), in order to obtain directly a fluid with non-newtonian (bulk) properties the complete solvent evaporation is required (6÷8 hours at 70÷80 C are typically enough). In Figure 2 and Figure 3 the morphological and rheological characterizations of several nanosilica wt% filled PEG solutions are respectively reported: in the SEM images the n-SiO$_2$/PEG chemical interaction is highlighted, while the viscosity/shear measurements (performed by parallel-plate rheometer) give evidence of the STF fashion as from 10wt% of nanosilica inclusion (showing the typical knee [5,9,10] at shear of about 10Hz) and a quasi-solid behavior for 15wt% and over loading.

Three textile materials have been treated with the different wt% loaded solutions realized. In Table 1 below their main characteristics are listed. XP Kevlar is highlighted to pick out its reference as starting best material in terms of density and claimed ballistic properties: this

advanced *DuPont* material is produced by not trivial polymeric/fiber intercalation treatment, resulting in high compact thin lightweight paper-like flexible structure. B Kevlar is a conventional typology of aramidic fiber woven, while hybrid KN material results from an experimental try to couple spongy waste Kevlar to commercial Nylon fabric.
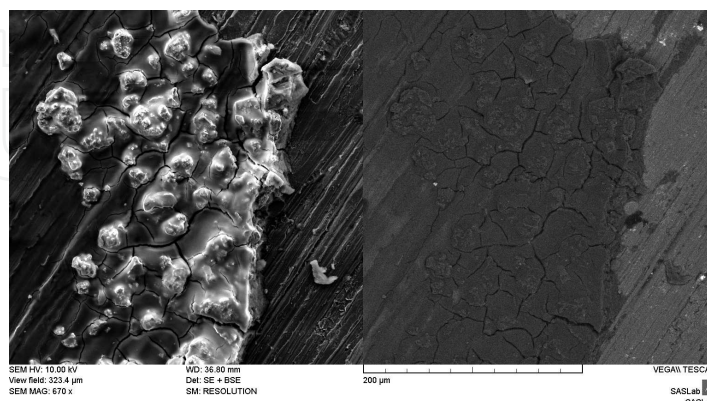


**Figure 2.** SEM photos of a drop-sample from a solution realized with n-SiO$_2$ at 20wt% inside PEG matrix after the ethanol evaporation. The SE image (left) shows the coupled morphology of the two chemical species, the correspondent BSE one (right) enhances the excellent mixture uniformity degree and the very low amounts of inner voids.
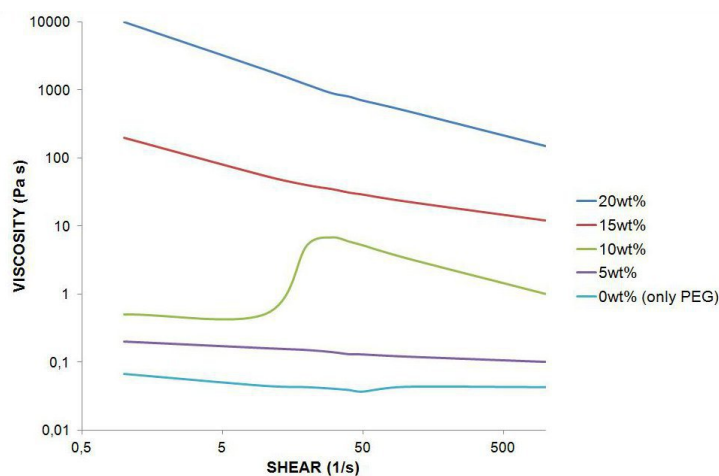


**Figure 3.** Viscosity/shear behavior of mixtures loaded with different weight percentages of nanosilica (measurements performed by parallel plate rheometer, shear 1 1/s to 1000 1/s, T 25 C): an evident phase transition (non newtonian behavior) is detectable around shear values of 10 Hz for the solution loaded at 10wt%.

The fabric impregnation with n-SiO$_2$/PEG mixtures diluted in solvent has to take place in relatively prompt way, in order to avoid unevenness treatment of the several layers due to potential physical/chemical changes of the post-sonicated solution (further solvent evaporation, filler sedimentation, cluster formation, etc.). For each kind of fabric and of mixture concentration the suitable fluid amount needed to achieve the maximum absorption is preliminary estimated. That is necessary because the highly diluted solutions saturate the fabrics with an

effective n-SiO$_2$/PEG absorption lesser than how potentially possible, as clear from halfway imbibitions and weight control operations. Such evaluation is performed by wetting drop by drop a layer of fixed dimensions until the first saturation, waiting for solvent evaporation in oven at 70÷80 C (considered run out when the weight reduction is less than 1% for measurements taken one hour apart), impregnating again and so on, until the dry layer weight has stabilized. For each kind of material the absorption properties (i.e. the weight increase) must be strictly linked to the results of the ballistic test, thus are reported in details in the experimental section. From a qualitative point of view, the following general considerations can be pointed out by visual inspection as well as SEM morphology investigations (Figures 4,5): very high concentration (>20wt%) mixtures reinforced fabric show a so poor manufacturing degree (Figures 4a-b), with the presence of a clotty gloss weakly attached to the layer surfaces; XP fabric is basically refractory to the treatment due to its above mentioned chemical composition, as clear from so low absorption rates and structure degradation phenomena (cfr. Figures 4c-d); B fabric shows the best behavior in terms of fibers-nanofluid interaction, resulting in highly uniform woven bulk structure (Figures 4e-f); KN fabric is treated only on the Kevlar side, which presents a tridimensional woven mat (Figure 5a) that assists the absorption mechanism (Figures 5c-d), while the hydrophobic Nylon backside surface (Figure 5b) doesn't show any kind of interaction with the fluid.

| material | symbol | areal density (kg/m$^2$) |
|---|---|---|
| *DuPont*™ Kevlar XP | **XP** | 0.51 |
| Saatilar batavia 4/4 | **B** | 0.62 |
| hybrid Kevlar-Nylon | **KN** | 0.65 |

**Table 1.** Main characteristics of the three Kevlar-based fabric tested.

The procedure of fabric impregnation consists in the simply dipping within a bowl filled with the suitable solution amount, then the layers are squeezed (Figure 6a) and put inside the oven for the solvent evaporation (typically 6÷8h at 70÷80 C, see Figure 6b). Finally, the treated layers are enveloped with polyethylene sheets (Figure 6c-d) in order to minimize the loss of material not perfectly stuck on the surfaces and to avoid unwanted interaction at the interfaces between neat/treated surfaces (lubrication or degradation of fluid incompatible fabrics). Fabric-reinforced flexibility has been discovered essentially unchanged comparing with neat material, even in the case of treatments with high concentration nanofluid mixtures.
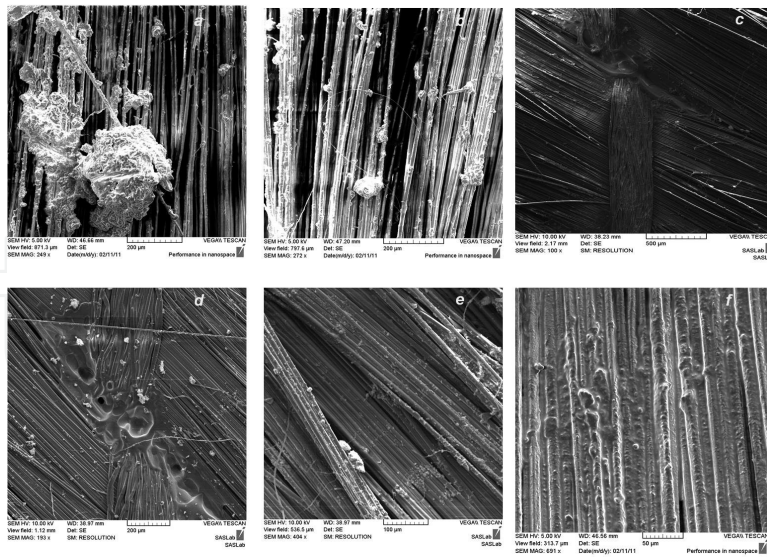
**Figure 4.** SEM images of neat/STF-reinforced fabrics: a)-b) B fabric treated with 50wt% STF solution; c) XP fabric neat morphology; d) XP fabric treated with 10wt% STF solution; e)-f) B fabric treated with 10wt% STF solution.
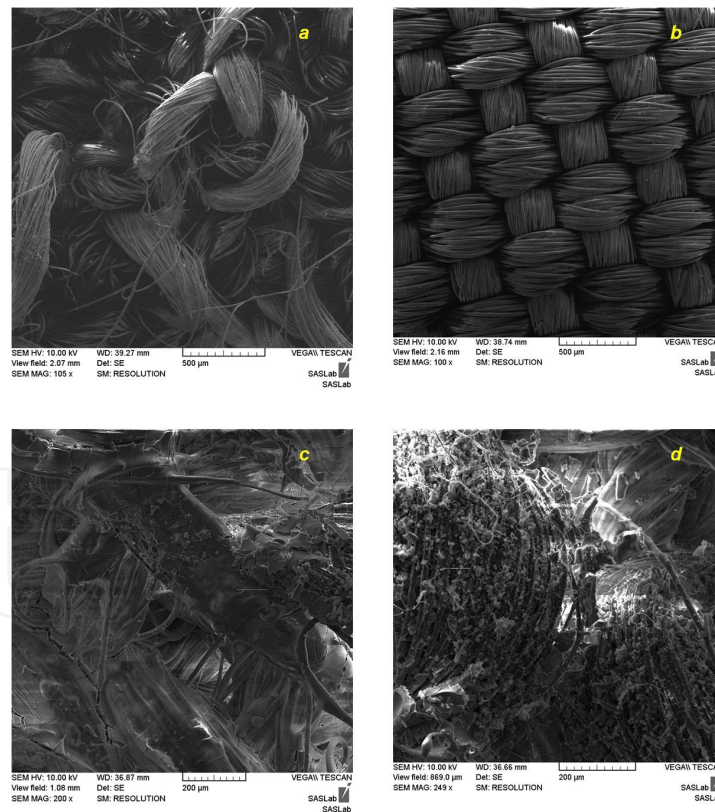


**Figure 5.** SEM images of neat/STF-reinforced fabrics: a) KN fabric neat morphology, Kevlar side; b) KN fabric neat morphology, Nylon side; c) KN fabric treated on Kevlar surface with 10wt% STF solution; d) KN fabric treated on Kevlar surface with 20wt% STF solution.

**Figure 6.** Different step of Kevlar-reinforced based antiballistic panels manufacturing: a) fluid application onto layers surface, b) solvent evaporation in oven, c) enveloping procedure, d) the panels ready for the ballistic test.

## 3. Experimental set-up

The ballistic characterization of the above described manufactured materials has been performed by means of an in-house built device called Coil Gun (CG), that is a typology of the more general electromagnetic accelerators equipment class. The idea to use intense electromagnetic pulses to exploit the intriguing matter/field interaction for propulsion applications is not so new, the first scientific researches in this area being carried out since many decades ago [4,11,12]. Several important results have been achieved in terms of ballistic performances, at the present time [13,14], anyway, the technological challenge is to reduce the system devices cost, weight and dimensions in order to compete with the conventional ballistic facilities. The CG basic background is the well known phenomenon of attraction suffered by a ferromagnetic body toward the middle of an hollow coil when a fixed current flows through this latter. As schematically depicted in Figure 7, the current flow produces an axial magnetic field inside the coil with maximum value (proportional to current intensity and coil turns number) around the coil central zone; the magnetic field decreases of about one half nearby the two coil's ends and goes rapidly to zero outside. A ferromagnetic object located not so far from one end of the coil suffers a strong magnetization (usually several order of magnitude greater than the magnetic

induction, due to the high magnetic permeability of ferromagnetic materials), thus resulting in an axial force depending in intensity and sign from the first derivative of the magnetic field [15]. In the case of a continuous steady current, the object's equilibrium position is clearly the center of the coil (i.e. where the body's center of mass fits to that of the coil), that is reached by friction after some (very fast) oscillations back and forth around the equilibrium center. If, on the contrary, an high current pulse is provided in such a way (i.e. with a characteristic time-constant) that the intensity falls to zero when the object is just coming to the coil's middle zone, then the backward recalling force is cut off and the object may move fast forward (and outside the coil) without kinetic energy loss. One simple way to obtain a pulse of current is to produce a capacitor discharge: a CG system thus works by exploiting a capacitor discharge across an inductance, that is via an RLC circuit discharge (Figure 8). In other words, the aim of the CG is to shoot a ferromagnetic bullet by converting the electrostatic energy stored in a capacitance into projectile's kinetic energy, thanks to the switch to magnetic energy inside an inductance coiled round the projectile's barrel.
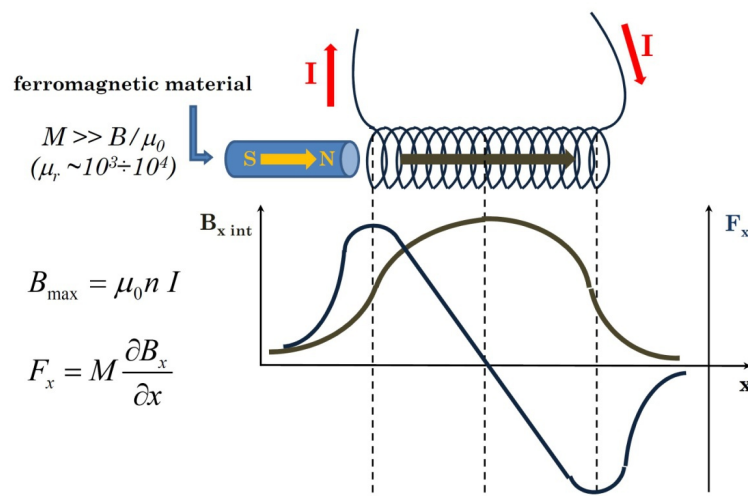


**Figure 7.** Coil Gun basic background: schematic representations and expressions of the magnetic field inside the coil due to the current flow, the induced magnetization of the ferromagnetic body, and the force acting on this latter.

The in-house built CG is shown in Figure 9: the main parts of the CG are the coil inductor, the projectile's barrel (that acts as support for the coil wrapping), the capacitors bank, the switch system, and the rectifier diodes. The coil inductor increases the acceleration of the projectile during its passage across itself. Its dimensions and turns number are crucial parameters; in fact, since the greater is the inductor turns number the higher is the inductance, then the electric discharge impulse rises, and above all decay time could result too much higher compared to the velocity of the projectile within the inductor. In such a case the efficiency of the CG could be compromised. The greatest efficiency is obtained when the impulse is shorter than the time took by the projectile to cross the half coil inductors length. If this condition is not satisfied then the inductors will apply an attractive force on the projec-

tile. This force will act in the opposite direction with respect to the projectile motion, thus decreasing the projectile acceleration. The diodes connected to the coil in the opposite polarity with respect to the capacitors are necessary to dump the negative voltage semi-wave oscillation caused by the capacitors discharge and inductors charge process. The dimensioning of the inductor and the capacitors must be computed in order to obtain the maximum efficiency. This means that the coil inductor should have the lowest time charge constant while the capacitors the fast discharge time constant. This is the fundamental condition required in order to avoid the forward-back projectile magnetic strength effect. In fact, once the projectile has overcome the half coil length, the back magnetic action strength starts to act on the projectile decreasing the initial forward acceleration imparted to the projectile. Since the capacitance discharge acts across the coil inductors, the best compromise can be found taking into account contemporary both the capacitance discharge constant time and the inductor charge one. Such a compromise can be obtained by reducing the coil inductor turns' number, as well as the capacitors' capacitance. Preliminary numerical simulations [16,17] have indicated that by a suitable arrangement of high capacitance ($4{\times}10^3\mu$F) capacitors as discharge trigger for a typical bullet/barrel system (mass projectile ~10g, gun length ~40cm), it's possible to reach values of 1÷2km/s for the bullet's speed, thanks to an effective coil propulsion force of by about $10^3$kN. By now the highest measured speed was near below 90m/s with capacitors of $12{\times}10^3\mu$F; next implementation will surely give the opportunity to come nearer the computed values. In such a case the device will be really appropriate for ballistic aerospace testing, by providing faithful results about the interaction between materials and space debris (~8km/s).
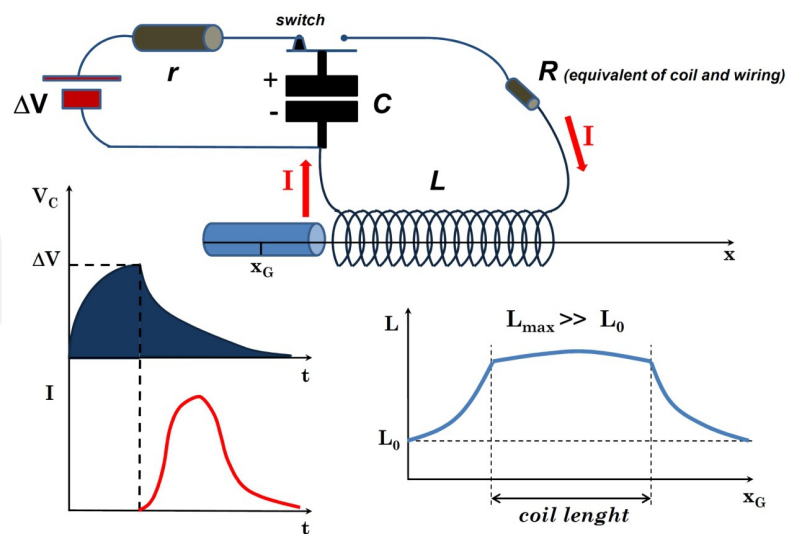


**Figure 8.** Coil Gun working: schematic representation of the RLC circuit (the charging phase concerns the r-C circuit, r being the capacitor loading resistance) with temporal behavior of capacitor voltage and intensity of current inside the coil. The qualitative variation of the circuit inductance highly dependent on the projectile's position during the discharge is also highlighted.
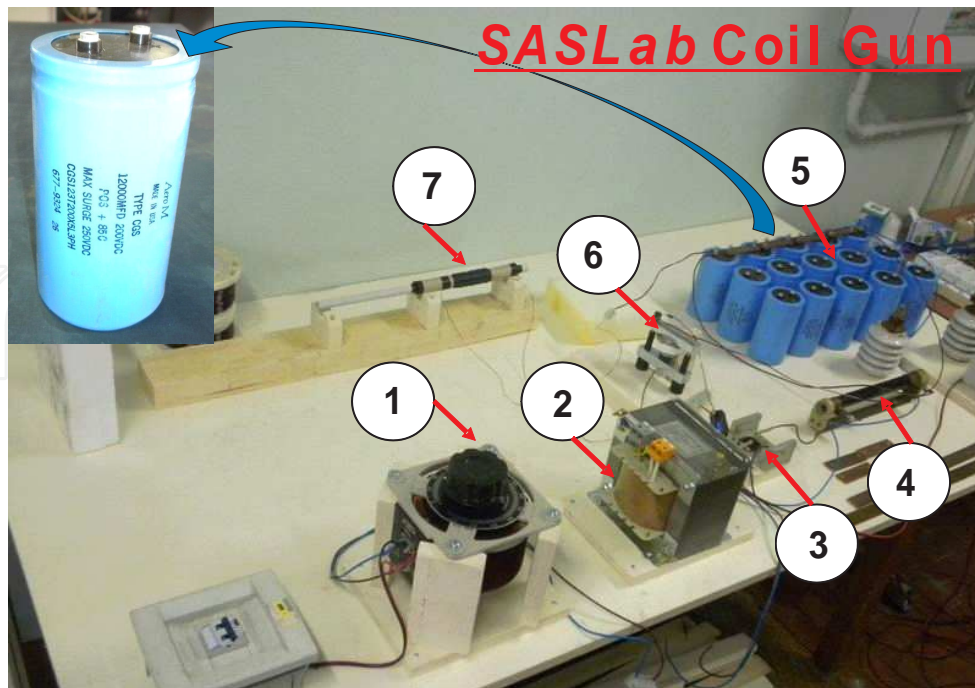
**Figure 9.** Picture of the Coil Gun system in-house realized (*SASLab-DIAEE* of *Sapienza* University): 1. Resistive Variac (V$_{input}$ 220 V, V$_{output}$ 0-250 V CA); 2. Transformer (V$_{input}$ 250 V, V$_{output}$ 1200 V CA, 1A); 3. Rectifier Diodes to convert AC in DC supply; 4. Resistor (1kΩ, 50W); 5. Capacitors (12000 μF, 200 V DC); 6. High power SCR (3000V$_{max}$, 300A); 7. CG inductor (copper coil winded on aluminum barrel).

It has to be pointed out, on the other hand, that any numerical approach toward the system optimization deals with a so complex analytical problem. In fact, the system of second order differential equations for the two time laws I(t) and x(t)

$$L \frac{d^2 I(t)}{dt^2} + R\frac{dI(t)}{dt} + \frac{1}{C}I(t) = 0$$

$$m\ddot{x}_G = F_x = M\frac{\partial B_x}{\partial x}[B_x = B_x[x;I(t)]] \qquad (1)$$

$$I(0) = 0 \quad V_c(o) = \Delta V$$

$$x_G(o) = x_0 \quad \ddot{x}_G(0) = 0$$

at first sight of relatively simple resolution (starting from the trivial expression of I(t) for RLC discharge), actually hides a tremendous non linear coupling due to the really appreciable variation of L during the discharge. The inductance of an hollow coil, as well known, can raise by several order of magnitude if a magnetic material is located inside the coil's core: since the body is magnetized (with M not constant too, since it depends on the magnetic field, i.e. on the current intensity) the circuit inductance is thus highly unsettled during the projectile's motion, with obvious consequences on the system time evolution. The modeling has thus to take into account for the physical changes of the fundamental parameters

$$M = M[I(t)]$$
$$L = L\left[x(t); M(I(t))\right]$$

(2)

so that the system (1) should be solved with an heuristic recursive approach, starting from the experimental measurements of velocity hereafter reported (Table 2). These latters are obtained by varying the charging applied voltage (at one's pleasure) and the CG macroscopic parameters (within the technical limits), that are: the iron bullets (S - length 8cm, diameter 6.3mm, mass 17.2g; L - length 16cm, diameter 6.3mm, mass 36.6g; see Figure 10a), the coils (A - wire diameter 2.1mm, length 15cm, 58 coils, 8 turns, $L_0$=1.54mH; B - wire diameter 3.2mm, length 14cm, 40 coils, 7 turns, $L_0$=0.55mH; see Figure10b-c), and the bank capacitors (C=12000μF) configuration (C1 - 5 C series, $C_{eq}$ = 2400μF; C2 - 2 C1 parallel, $C_{eq}$ = 4800μF; C3 - 3 C1 parallel, $C_{eq}$ = 7200μF). The gun barrel is kept fixed (aluminum tube: length 31.6cm, outer diameter 10mm, inner diameter 7.6mm), the speed measurements are recorded by means of a ballistic chronograph (*ProChrono* chronograph, minimum speed 17m/s, precision 0.5m/s; see Figure 10d), the results are averaged over five shots for each arrangement.



**Figure 10.** CG set-up pictures: a) short (S) and long (L) iron bullets; b) different copper coils tested; C) inductance static measurements by *Agilent* LCR Meters; d) ballistic *ProChrono* chronograph for bullet's speed measurements.

| | BULLET SPEED (m/s) | | | | | | | |
|---|---|---|---|---|---|---|---|---|
| d.d.p. | *COIL A* | | | | | | *COIL B* | |
| (Volts) | C1 | | C2 | | C3 | | C3 | |
| | S | L | S | L | S | L | S | L |
| *350* | - | - | <17 | - | 22.2±0.7 | <17 | 33.1±1.1 | 27.1±1.1 |
| *400* | - | - | 19.5±0.7 | - | 23.5±0.6 | 17.1±1.1 | 37.1±1.1 | 32.1±1.1 |
| *460* | - | - | 23.3±0.6 | - | 24.5±0.6 | 17.6±0.6 | 40.0±1.5 | 35.2±1.0 |
| *500* | - | - | 25.2±0.8 | - | 25.1±0.4 | 19.1±0.8 | 43.5±1.3 | 38.4±1.0 |
| *550* | <17 | - | 27.7±0.6 | - | 25.0±0.6 | 22,7±1.0 | 45.9±1.2 | 42.8±1.3 |
| *600* | <17 | - | 28.5±0.6 | <17 | 24.2±0.5 | 25.0±0.6 | 49.2±1.2 | 48.5±1.2 |
| *660* | <17 | - | 30.0±0.6 | <17 | 23.6±0.6 | 28.1±0.7 | 53.1±1.2 | 55.6±1.1 |
| *700* | 18.1±1.8 | - | 31.3±0.7 | <17 | 23.0±1.0 | 29.5±0.9 | 55.3±1.5 | 61.6±1.2 |
| *750* | 19.5±1.3 | - | 31.5±0.8 | 19.3±1.3 | 22.3±1.1 | 31.5±0.8 | 57.2±1.5 | 68.3±1.1 |
| *800* | 21.7±1.2 | <17 | 32.1±0.6 | 27.1±1.2 | 20.5±1.2 | 32.6±0.6 | 58.8±1.4 | 74.9±1.0 |
| *850* | 24.6±0.9 | <17 | 32.4±0.5 | 29.4±1.1 | 19.1±1.7 | 33.3±0.5 | 59.5±1.3 | 80.3±0.7 |
| *900* | 26.5±0.8 | <17 | 32.2±0.8 | 32.7±1.1 | <17 | 34.2±0.5 | 59.2±1.3 | 84.1±0.5 |
| *950* | 29.9±1.0 | 25.4±1.3 | 31.5±1.0 | 35.3±0.9 | <17 | 34.5±0.3 | 58.1±1.0 | 86.0±0.4 |
| *1005* | 31.5±0.8 | 31.5±1.0 | 31.2±1.0 | 37.1±0.7 | <17 | 34.0±0.5 | 55.4±1.1 | 85.7±0.6 |
| *1050* | 33.1±0.7 | 35.2±0.5 | 30.5±1.1 | 37.5±0.5 | - | 33.3±0.6 | 50.3±1.5 | 82.5±0.8 |
| *1095* | 34.2±1.0 | 38.9±0.7 | 29.3±1.1 | 37.3±0.6 | - | 31.5±0.7 | 42.2±1.4 | 78.5±0.8 |

**Table 2.** Speed measurements at different input voltages for the several CG arrangements tested.

The several trends of the bullet's speed depending on the input voltage for the different arrangements highlight the intriguing, complex and highly non linear behavior of the system with respect to its physical main parameters. A first preliminary analysis of the experimental results listed in Table 2 and outlined in Figure 11 stresses in fact the not obvious dependence between the several variables involved, mainly between the time charge/discharge circuit response and the mass of the bullet. The bell-shaped curves demonstrate that the energetic system balance, defined by

$$\eta = \frac{K}{E_C} \qquad \left( E_C = \frac{CV^2}{2} \quad , \quad K = \frac{mv^2}{2} \right) \tag{3}$$

with obvious physical meaning of the symbols, doesn't follow a trivial trend (speed increasing for higher voltages). It's clear, for example, that for coil A, with the bullets adopted and around the maximum voltage that can be applied to not more than five capacitor in series

(each one can be charged up to 250V), the system efficiency raise up by decreasing the total capacitance, thus supplying less energy to the system ($E_c$): from (3) one can find a best efficiency $\eta \sim 2\%$ for LAC1 configuration at the maximum voltage.
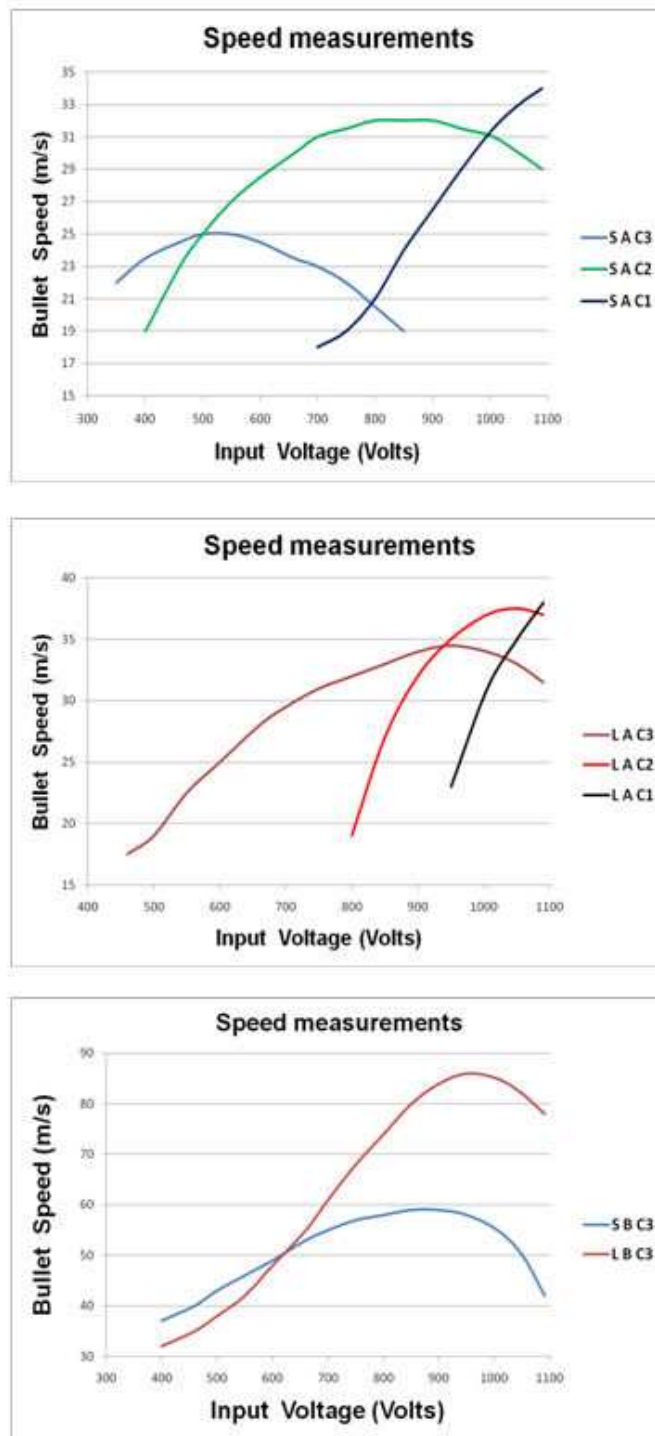


**Figure 11.** Graphic representations of the speed measurements reported in Table 2.

For coil B in C3 configuration, on the other hand, the heavier L bullets results faster than the lighter S over almost the whole voltage range, with maximum efficiency η ~ 4.5% around 850V. Such results, of course, are connected to the time employed by the bullets to reach the coil center, over which they are recalled back, as explained above. To get higher speed and efficiency all the parameters have to be accurately matched: the results obtained for coil B and bullet L suggest that a suitable arrangement of capacitors bank may let one able to raise the bullet's speed up to 100m/s only with the present Coil Gun stage. Anyway, to perform an as precise as possible material ballistic characterization, a good test reproducibility rather than higher bullets kinetic energies has been addressed by now. With such aim, two fixed configurations with the lowest statistical dispersions in terms of bullets velocities were chosen: LAC3 and LBC3 both at 950V, in what follow related to the low energy (~22J) and high energy (~135J) test respectively. By watching at the experimental error values in Table 2, in fact, it's clear that it's worth operating around maximum points of the curves of Figure 11 in order to avoid ballistic characterization mismatches as much as possible. Furthermore, the use of the longer bullet ensures more stable conditions about the relevant error source due to the bullet initial position: in fact, the coil inductance increases appreciably even with a not magnetized (metallic) body inside its core (changes up to 6÷8 times were found by inductance static measurements performed by inserting both bullets, partially and totally, inside the coil; cfr. Figure 10c), thus resulting in speed changes for same coil/bullet/capacitance arrangements at same input voltages (Figure 12) that cannot be neglected.
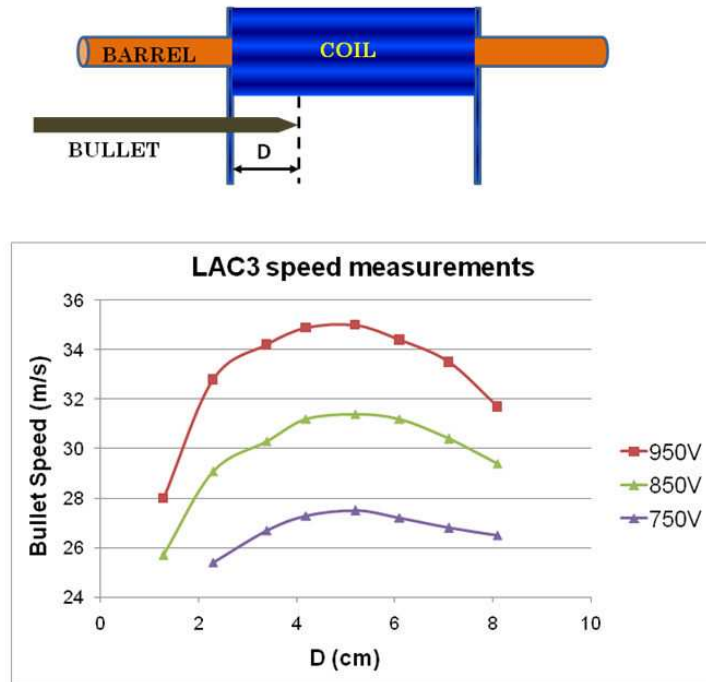


**Figure 12.** Bullet velocity versus initial position: the measurements performed in the same arrangement (LAC3) for three different input voltages showed that the CG efficiency may considerably change by few millimeters shift of bullet initial positioning.

## 4. Results and discussion

In this section the most significant results of the ballistic characterization of the nanofluid-reinforced Kevlar-based fabric by means of the CG device are reported and discussed. The choice of the test panel configurations (layers type and number, target surface, alternation and coupling between neat and treated layers, assembling modality, etc.) has been first suggested by the experimental set up best solutions, beyond the purpose to obtain performances similar or even better than the best reference samples in terms of weight/resistance ratio. Preliminary characterization test of the experimental apparatus have indicated the most suitable ensemble of physical parameters (bullet typology, shot energies, gun-target distance, etc.) in order to achieve the best compromise between test efficacy and reproducibility. In particular, the combined constraints of gun and projectile's direction stability during the shot to obtain a 90 central impact on the targets have suggested to keep the sample surface dimensions inside 20×20cm (such value was further lowered cause the big quantity of fluid required to carry out a significant number of experimental test). In Figure 13 the experimental set up adopted is schematically depicted: the samples are fixed by elastic clamps to the wood support, where a plasticine witness is centrally positioned (Figure 14) to estimate the different panel performances in terms of absorbed energy.
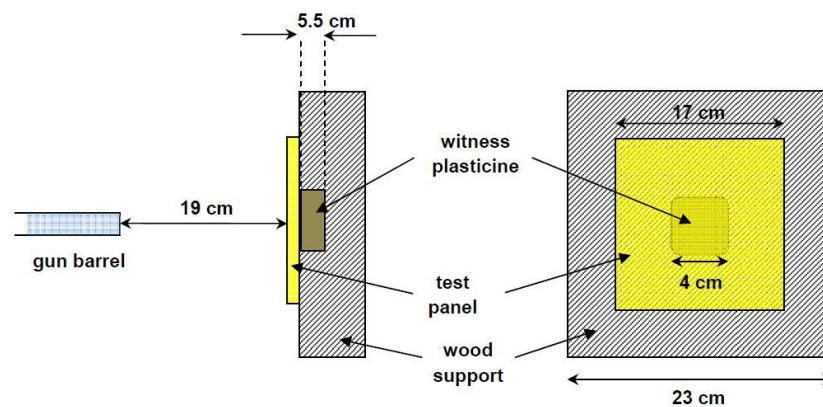


**Figure 13.** Panels ballistic characterization test by CG: schematic lateral (left) and frontal (right) views of the adopted set-up.

About the layers number, the investigation has been oriented by the reference fabric (neat XP) performances: the number of layers was set to eleven, such to obtain a precise quantitative evaluation of its ballistic properties with the operating experimental conditions. As a consequence, the prototype panel configurations have been established by taking into account most of all the panel total weight requirements, in order to carry out a reliable comparison. For the same reason the results obtained with high (>20wt%) STF concentration have not been taken into consideration, since the critical manufacturing issues due to over-filled solutions produce not homogeneous structures and thus a poor test reproducibility (beyond a not practically useful material). Direct measurements and evaluations for several

panel configurations are summarized in Table 3 below, the results being averaged over five shots for each ballistic test. For each panel typology are indicated symbol, layers sequence (following the nomenclature of Table 1 for the fabric type, and subscribing the STF concentration for the treated materials), and total weight (P); for the two low/high energy test above defined the measured penetration depth in the plasticine witness (L), and the computed relative absorbed energy in percentage ($\Delta E$) and efficiency (Q) are then reported. The penetration depth is measured by depth gauge (precision 0.05mm, see Figure 15), the relative absorbed energy and efficiency are simply defined as follow

$$\Delta E = \frac{L_0 - L}{L_0}, \ Q = \frac{\Delta E}{P} \tag{4}$$

where $L_0$ indicates the penetration depth into the plasticine witness without sample (low energy test: $L_0 = 9.2$ mm; high energy test: $L_0 = 50.8$ mm). The absorbed energy is an index of the intrinsic ballistic effectiveness of the tested material, while the efficiency factor represents, by weighting on the material density, a balanced evaluation of the global material properties in view of applications in which both lightness and resistance are contemporaneously required.



**Figure 14.** Picture of the plasticine witness located in the square hole of the sample's support in front of the CG barrel.

By analyzing the numerical results of Table 4 the effectiveness of the fabric reinforcement treatment by the STF solutions realized is evident at first sight: the performances of every blank typology ($b_0$, B and KN) are improved by the corresponding STF-reinforced configurations in terms of absorbed energy. Moreover, the higher is the nanosilica concentrations within the STF solutions, the greater is the percentage of absorbed energy, as shown in Figure 16, thus enhancing the direct role of reinforcing element played by the n-SiO$_2$ based nanofluids when coupled to B and KN type fabrics. That is supported by the observation of the zone perforated by the bullets: a more collective resistance work done by the fibers of

the reinforced fabric comparing to the neat one is detectable in the panels backside images after the shot (Figure 17), as well as in the SEM photos of the impact point (Figure 18).

| | panel typology | | low energy test (~22J) | | | high energy test (~135J) | | |
|---|---|---|---|---|---|---|---|---|
| symbol | configuration | P (g) | L (mm) | ΔE | Q | L (mm) | ΔE | Q |
| XP | 11 XP | 175 ± 2 | 1.2 ± 0.2 | 87% | **0.50** | 10.8 ± 0.5 | 79% | **0.45** |
| $b_0$ | 1 XP / 9 B / 1 XP | 284 ± 5 | 5.8 ± 0.3 | 37% | **0.13** | 36.0 ± 1.1 | 29% | **0.10** |
| $b_0$* | 1 XP / 9 $B_{15}$ / 1 XP | 319 ± 8 | 5.1 ± 0.3 | 45% | **0.14** | 29.3 ± 1.0 | 42% | **0.13** |
| B | 5 XP / 3 B / 1 XP | 180 ± 4 | 5.5 ± 0.4 | 40% | **0.22** | 34.1 ± 0.4 | 33% | **0.18** |
| $B_{10}$ | 5 XP / 3 $B_{10}$ / 1 XP | 192 ± 6 | 5.3 ± 0.3 | 42% | **0.22** | 31.5 ± 0.5 | 38% | **0.20** |
| $B_{15}$ | 5 XP / 3 $B_{15}$ / 1 XP | 196 ± 4 | 4.8 ± 0.3 | 48% | **0.24** | 27.6 ± 0.6 | 46% | **0.23** |
| $B_{20}$ | 5 XP / 3 $B_{20}$ / 1 XP | 199 ± 5 | 4.1 ± 0.2 | 55% | **0.28** | 22.8 ± 1.1 | 55% | **0.28** |
| KN | 5 XP / 4 KN / 1 XP | 184 ± 3 | 5.2 ± 0.3 | 43% | **0.24** | 33.1 ± 0.7 | 35% | **0.19** |
| $KN_{10}$ | 5 XP / 4 $KN_{10}$ / 1 XP | 199 ± 6 | 4.3 ± 0.2 | 53% | **0.27** | 26.0 ± 1.0 | 49% | **0.25** |
| $KN_{15}$ | 5 XP / 4 $KN_{15}$ / 1 XP | 203 ± 4 | 3.2 ± 0.3 | 65% | **0.32** | 18.2 ± 0.5 | 64% | **0.32** |
| $KN_{20}$ | 5 XP / 4 $KN_{20}$ / 1 XP | 205 ± 4 | 1.9 ± 0.2 | 79% | **0.39** | 10.5 ± 0.6 | 79% | **0.39** |

**Table 3.** Table 3. Ballistic characterization results (the horizontal blocks enclose the results for single groups of blank/ treated materials).

Such improvements are confirmed by the Q-factor trend, even if in a less effective way: the more concentrated solution raise the fabric saturation level in terms of weight increasing, thus lowering the panel global efficacy. In particular the Q values founded for the $b_0$ type panels give evidence of the drawbacks due to an overall utilization of the STF treatment, because the structure heaviness may offset the gain in impact resistance capability. For this reason the mix configurations with the first 5 layers made of neat XP were designed: as best reference material, the XP Kevlar has confirmed the better weight/resistance trade-off in these experimental conditions. On the other hand, as mentioned in the first section, the poor

coupling between STF and XP doesn't give any contribution to the fabric's resistance, rather degrading the fibers structure. As far as the impact energy is concerned, an interesting property of the STF-based samples can be noticed: the quasi-unchanged ΔE and Q values of the reinforced panels (mainly of those with higher nanofiller wt%) in the two different energy range test, with respect to the correspondent lowering discovered in the neat samples. That is highlighted by the crossing around 20wt% of the two curve pairs (B type and KN type) in the graphic of Figure 16, while in the starting points (0wt%, i.e. neat panels) the ΔE values are well spaced, even for the best configuration (horizontal reference lines).
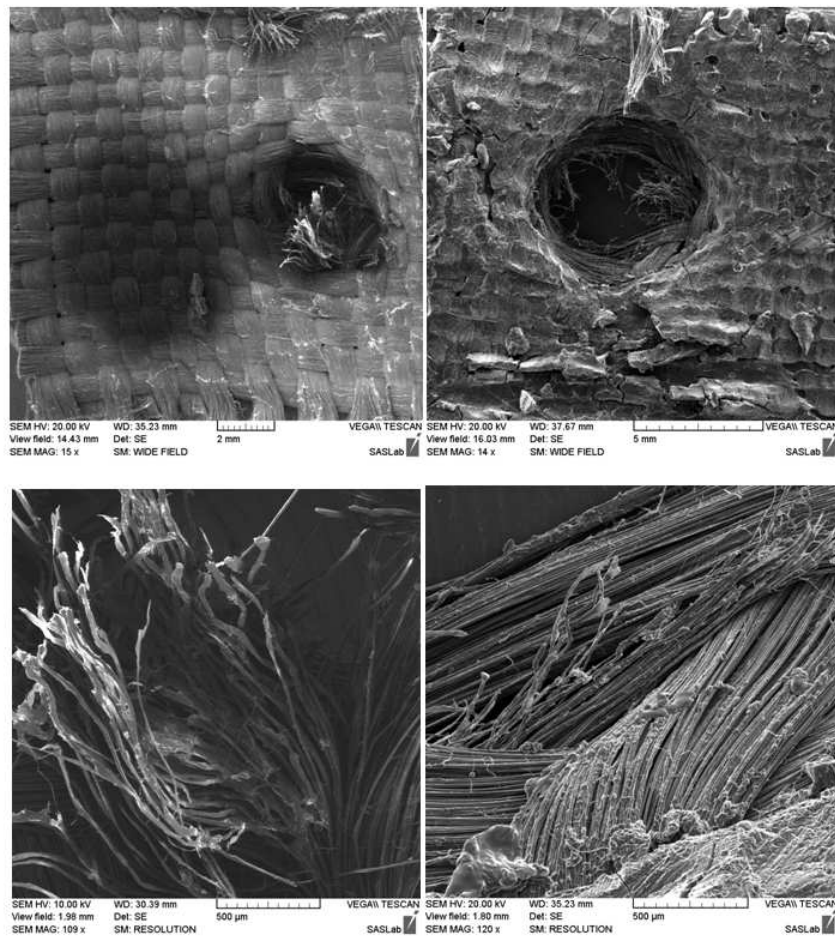


**Figure 15.** Pictures of a panel sample just after the ballistic test.
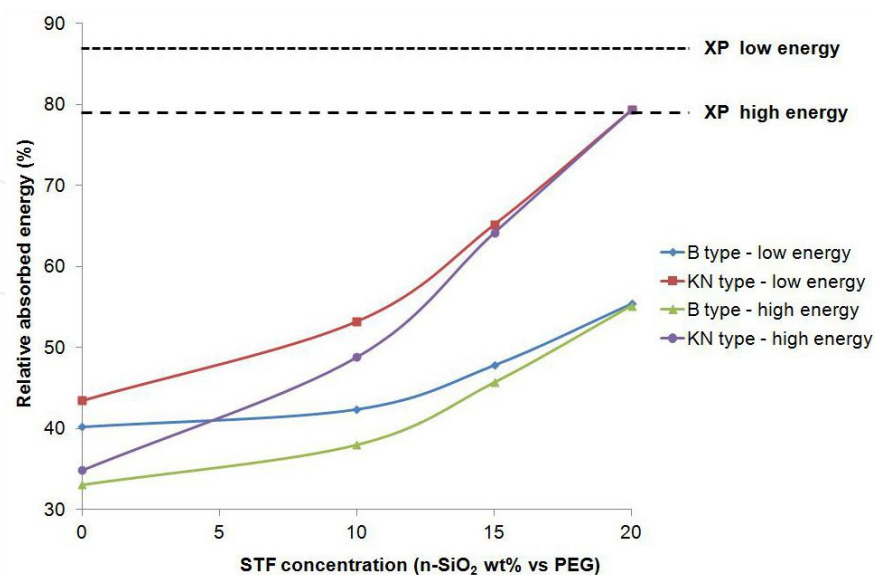


**Figure 16.** Absorbed energy dependence on nanoparticles wt% inside the several typologies of STF-reinforced fabric panels.
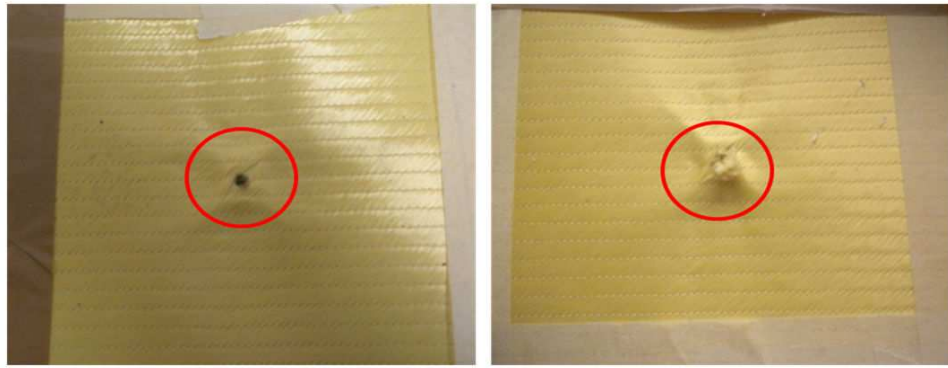
**Figure 17.** Backside (exit wound) pictures of a B (left) and a $B_{20}$ (right) configuration panel samples after the low energy test.



**Figure 18.** Low (up) and medium (down) magnification SEM photos of the impact zone in B (left) and $B_{20}$ (right) configuration panel samples after the low energy ballistic test.

Such results suggest an intriguing fashion of the impact resistance mechanism by the STF-treated materials. In a very simplified scenario, a conventional structure puts up resistance

by a constant friction, so that the L quantities in (4) only depend on the intrinsic material properties: by this way the absorbed energy may be written as

$$\Delta E = \frac{E_{INC} - E_F}{E_{INC}} \tag{5}$$

where $E_{INC}$ and $E_F$ are the incident bullet's energy and the friction physical work respectively: if this latter is approximately constant (i.e. not dependent on the impact energy), the relative absorbed energy is clearly reduced by increasing the bullet's kinetic energy. In the energy range investigated this latter description seems to be reasonable for what concerns the untreated samples. On the contrary, the experimental results obtained for the treated fabric-based panels indicate a more complex mechanism of interaction (cfr. Figure 19), able to raise the friction effect (i.e. the fabric response upon impact) at higher incident energies. This feature may be so promising, mainly for the globally good performances of the treated KN-based type panels. In this case, in fact, the nanofluid/fabric suitable coupling (due to the particular fabric morphology) enhances the STF behavior: that makes this kind of structure (at the highest concentration wt%) competitive with the reference one, even matching it in the high energy range in terms of impact absorption. The next steps of the research has to be then addressed to the further upgrade of the treated KN-based structures, in particular for what concerns the manufacturing reliability of high percentage STF-filled materials.
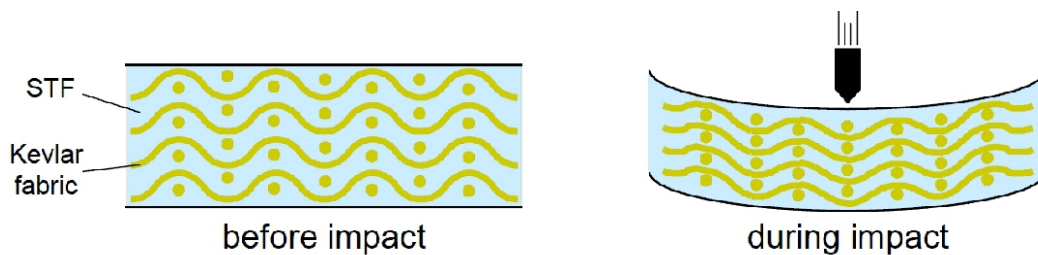


**Figure 19.** Schematic representation of elastic-like mechanical behavior of STF-reinforced Kevlar fabric upon a projectile impact.

## 5. Conclusions

In the present study the possibility to employ nanoparticles-based shear thickening fluid for improving the antiballistic properties of Kevlar fabrics has been investigated. Nanosilica particles have been used to realize the reinforcing solutions, and an electromagnetic accelerator device called Coil Gun has been designed, realized and characterized to perform ballistic impact tests on several type of Kevlar-based panels. The fabric samples realization modality consists essentially of two phases: the nanofluid preparation and the fabric impregnation treatment. The first one has to be accurately defined, in order to be confident of the basic effectiveness of the proposed reinforcing material: with such an aim, the combina-

tion of the main parameters (material amount percentages, mixing techniques, solvent influence, etc.) affecting the nanofluid preparation have been analyzed, and the several solutions characterized in terms of their rheological properties (viscosity/shear). The second one is strictly dependent on the physical/chemical coupling at the nanofluids/fabric interface: the macroscopic indications provided by the manufacturing procedure, as well as the morphological characterization analyses of the fabric surfaces, have suggested to employ two particular typologies of Kevlar fabric reinforced with nanofluid solutions with concentrations up to 20wt%. The in-house built Coil Gun has been carefully characterized in terms of its main parameters (bullets velocity, energy efficiency, system stability, etc.): two particular configuration (low/high energy) have been established for the fabric ballistic characterization, so that two different impact energy ranges have been investigated and, at the same time, the maximum test reproducibility has been achieved. The results obtained have outlined a better resistance upon impact provided by the highest concentrations of nanofluid-reinforced materials against the corresponding unreinforced ones, thus suggesting further implementation of such nano-reinforced fabrics for antiballistic applications. In particular, a not conventional impact response mechanism seems to be dependent on the nanofluids employment, enhancing their effectiveness for energy increasing: such result can make the treated fabrics able to reach, and eventually overcome, the performances of the best commercial Kevlar-based material (here taken as reference). With such an objective, several technical improvements have to be supplied to the present state of art. Firstly, the manufacturing technique has to be optimized in order to realize fabrics reinforced by higher concentrations of nanofluid solutions: the experimental results have shown, in fact, a clear influence of the nanosilica percentage of inclusion on the fabric absorbing energy capability. This goal, of course, has to be addressed without lack of material homogeneity and flexibility, in order to realize prototype materials of practical application. Secondly, a Coil Gun implementation in terms of efficiency is needed, in order to explore different (higher) energy ranges with the same degree of test reproducibility. Such step will be needful for achieving a deeper knowledge of the underlying impact response mechanism showed by the nanofluid-based material, thus giving the opportunity for their further optimization in terms of antiballistic performances.

## Author details

Roberto Pastore, Giorgio Giannini, Ramon Bueno Morles, Mario Marchetti and Davide Micheli

Astronautic, Electric and Energetic Engineering Department, University of Rome "Sapienza", Rome - Italy

# References

[1] Mangalgiri, P. D. (1999). Composite materials for aerospace applications. *Bulletin of Materials Science*, 22(3), 657-664.

[2] Njuguna, J., & Pielichowski, K. (2003). Polymer Nanocomposites for Aerospace Applications. *Advanced Engineering Materials*, 5(11), 769-778.

[3] Micheli, D., Apollo, C., Pastore, R., & Marchetti, M. X. (2003). Band microwave characterization of carbon-based nanocomposite material, absorption capability comparison and RAS design simulation. *Composites Science and Technology*, 70(2), 400-409.

[4] Haghmaram, R., & Shoulaie, A. (2004). Study of Traveling wave Tubular Linear Induction Motors. *International Conference on power System Technology, POWERCON, November 21-24, 2004, Singapore.*

[5] Hassan, T. A., Rangari, V. K., & Jeelani, S. (2010). Synthesis, processing and characterization of shear thickening fluid (STF) impregnated fabric composites. *Materials Science and Engineering A*, 527, 2892-2899.

[6] Egres, R.G, Lee, Y.S., Kirkwood, J.E., Kirkwood, K.M., Wetzel, E.D., & Wagner, N.J. (2004). Liquid armor": protective fabrics utilizing shear thickening fluids. *IFAI 4th International Conference on Safety and Protective Fabrics, Pittsburgh, PA.*, 26-27.

[7] Wetzel, E. D., & Wagner, N. J. (2004). Stab Resistance of Shear thickening Fluid (STF)-Kevlar Composite for Body Armor Applications. *24th Army Science Conference, December 2, Orlando, FL.*

[8] Decker, M. J., Halbach, C. J., Nam, C. H., Wagner, N. J., & Wetzel, E. D. (2007). Stab resistance of shear thickening fluid (STF)-treated fabrics. *Composite Science and Technology*, 67, 565-578.

[9] Maranzano, B.J., & Wagner, N.J. (2001). The effect of interparticle interactions and particle size on reversible shear thickening: hard-sphere colloidal dispersions. *Journal of Rheology*, 45-1205.

[10] Lee, Y. S., & Wagner, N. J. (1983). Dynamic properties of shear thickening colloidal suspension. *Rheologica Acta*, 42, 199-208.

[11] Lell, P., Igenbergs, E., & Kuczera, H. (2003). An electromagnetic accelerator. *Journal of Physiscs E*, 16, 325-330.

[12] McNab, IR. (2003). Launch to space with an electromagnetic railgun. *IEEE Transaction on magnetic*, 39, 295-304.

[13] Schmidt, E., & Bundy, M. (2005). Ballistic Launch to Space. Vancouver BC, Canada. *International symposium on Ballistics*, 14-18.

[14] Shope, S., Alexander, J., Gutierrez, W., Kaye, R., Kniskern, M., Long, F., Smith, D., Turman, B., Marder, B., Hodapp, A., & Waverik, R. (2003). Results of a study for a

long range coilgun naval bombardment system. *Sandia National Laboratories, Albuquerque, NM 87185.*

[15] Purcell, E.M. (1965). *Electricity and Magnetism*, Mc Graw-Hill book Company, U.S.A.

[16] Micheli, D., Apollo, C., Pastore, R., & Marchetti, M. (2010). Ballistic characterization of nanocomposite materials by means of "Coil Gun" electromagnetic accelerator. *XIX International Conference on Electrical Machines- ICEM, Rome, Italy.*

[17] Micheli, D., Pastore, R., Apollo, C., & Marchetti, M. (2011). *Coil Gun electromagnetic accelerator for aerospace material anti-ballistic application.*, 1826-4697.